Pergamon

Int. J. Heat Mass Transfer. Vol. 38, No. 10, pp. 1879–1891, 1995

0017-9310/95 $9.50+0.00

0017-9310(94)00298-3

Turbulent natural convection and conduction in enclosures bounded by a massive wall

R. BEN YEDDER and E. BILGEN†

Mechanical Engineering Department, Ecole Polytechnique, University of Montreal, C.P. 6079, "City Center", Montreal, Quebec, Canada H3C 3A7

(*Received* 3 *May* 1994 *and in final form* 24 *August* 1994)

Abstract—Turbulent natural convection and conduction in enclosures bounded by a massive wall is numerically studied. Two-dimensional equations of conservation of mass, momentum and energy, with the Boussinesq approximation and using the κ–ε model for turbulence, are solved using a finite difference method. Grids are generated in a nonuniform manner so that steep gradients near the wall regions are accounted for as required. Various parameters were: Rayleigh number (from 10^8 to 10^{12}), dimensionless conductivity of bounding wall (from 1 to 10), dimensionless wall width (from 0 to 0.5), enclosure aspect ratio (from 0.5 to 1) and the inclination angle (from 0 to 180°). The results are reduced in terms of the normalized Nusselt number as a function of the Rayleigh number, and other dimensionless parameters. The isotherms and streamlines are produced for various Rayleigh numbers and geometrical conditions.

INTRODUCTION

Natural convection of fluid media in enclosures has received considerable attention over the past few decades, largely due to a wide variety of applications, which include building technology, electronic boxes, solar collector technology, energy storage, nuclear reactor technology, etc. Comprehensive reviews of natural convection have been documented in the literature [1, 2]. Most of the previous studies has addressed laminar natural convection in cavities bounded with rigid walls with zero thickness subjected to various boundary conditions. In many applications, the enclosure is bounded by walls with finite thickness and conductivity, which affect the natural convection in the enclosure. In addition, the Rayleigh number characterizing the flow mode often exceeds the critical values when the heat flux from the side wall is high, and the flow becomes turbulent. As a special case, enclosures with one bounding wall are encountered when simulating building components. For example, in direct gain passive solar systems, the dwelling is simulated as a two-dimensional enclosure having two vertical walls, one transparent and the other massive, which are bounded by two horizontal insulated boundaries. Heat transfer by a constant heat flux through the transparent vertical wall simulates solar radiation reception while an isothermal condition exists at the outer boundary of the massive wall, the adjacent building component at constant temperature.

Heat transfer by natural convection in these systems constitutes a major study area. The heat transfer by laminar natural convection was studied earlier [3]. Heat transfer by turbulent natural convection for these problems is not available in the literature. A literature review on buoyancy driven turbulent flow in enclosures and turbulence models used follows.

Various authors have studied the problem of the differentially heated square cavity. Markatos and Pericleous [4] obtained results for Rayleigh numbers ranging from 10^3 to 10^{16}: air was the fluid considered but the buoyancy term in the ε equation was omitted and density was considered proportional to $1/T$, avoiding the use of the Boussinesq approximation. They switched to turbulence at $Ra > 10^6$, invoked experimental observations to explain their decision and used their observation to derive Nu–Ra correlations. Thompson *et al.* [5] investigated the solution for the double glazing problem and their results show the correct qualitative behaviour, namely a thin boundary layer and a stratified, almost stagnant core. They used a prescribed eddy viscosity turbulence model and κ–ε model with wall function, though little detail has been given concerning coefficients and functions used near the wall, and concluded that the former model could give a good insight with little cost. Henkes *et al.* [6] provided a comparison between various turbulence models and found $Ra_{cr} \sim 10^9$ for air. They used geometric functions to refine the grid near the boundaries. No assumptions for the flow were made, except for the Boussinesq approximation.

Other studies are concerned about forced convection in confined cavities [7, 8]. They used the standard wall function in the κ–ε model, which is appropriate since the empirical constants are derived from forced flows.

It appears from these studies and others [9, 10] that various problems arise in predicting internal buoyancy flow. Furthermore, studies in the literature are

† Author to whom correspondence should be addressed.

NOMENCLATURE

A	aspect ratio, H/L
g	acceleration due to gravity [m s^{-2}]
h	convection coefficient [W m^{-2} K^{-1}]
H	cavity height [m]
k	thermal conductivity [W m^{-1} K^{-1}]
k_r	thermal conductivity ratio (k_w/k_f)
L	cavity width [m]
Nu	Nusselt number (hL/k)
p	dimensionless pressure
Pr	Prandtl number, ν/α
q	heat flux [W m^{-2}]
Ra	Rayleigh number ($g\beta qL^4/k\nu\alpha$)
S	source term
t	time
T	temperature [K]
u, v	dimensional velocity in x and y direction
W	dimensionless wall thickness
w	width of the bounding wall [m]
x, y	Cartesian coordinates
Δy	increment in the y direction.

Greek symbols

α	thermal diffusivity [m^2 s^{-1}]
β	thermal expansion of fluid [1/K]
δ	dimensionless distance from the wall (δ^*/L)
ε	dimensionless dissipation rate
θ	dimensionless temperature
κ	dimensionless kinetic energy
λ	dimensionless viscosity ratio (μ_w/μ_f)
μ	dynamic viscosity [kg m^{-1} s^{-1}]
ν	kinematic viscosity [m^2 s^{-1}]
ρ	fluid density [kg m^{-3}]
σ	correction factor in the κ–ε model
φ	angle of inclination, degrees
χ	empirical constant; equation (10)
ψ	stream function.

Superscripts

*	dimensional variables
+	distance from the wall; equation (10).

Subscripts

e	equivalent properties
f	fluid
max	maximum
o	reference value
p	first point near the wall
t	turbulent quantities
τ	tangential properties near the wall
w	wall.

for the case of isothermal vertical boundaries with no wall thickness, i.e. no conduction heat transfer.

Natural convection in enclosures has gained popularity in the past 10 years both due to the numerous applications derived from this configuration and for academic reasons, for example, bench mark solutions. Unfortunately, these studies are limited to the prediction of laminar flow in part because of the uncertainties related to the modelling of turbulence and the cost of such investigations. The present study models the turbulent natural convection in the cavity systems with a bounding massive wall.

PROBLEM DESCRIPTION

The system is shown in Fig. 1. It is an enclosure bounded by a massive wall with a finite conductivity on the right. A constant heat flux is imposed on the side opposing the massive wall to simulate solar radiation input and a constant temperature on the outer surface of the massive wall. The horizontal boundaries are adiabatic. It is assumed that the dimension in the z' direction is large enough and the end effects on the flow are negligible on the flow, i.e. the flow is two-dimensional. Experimental evidence suggests that this is, in fact, the case [11].

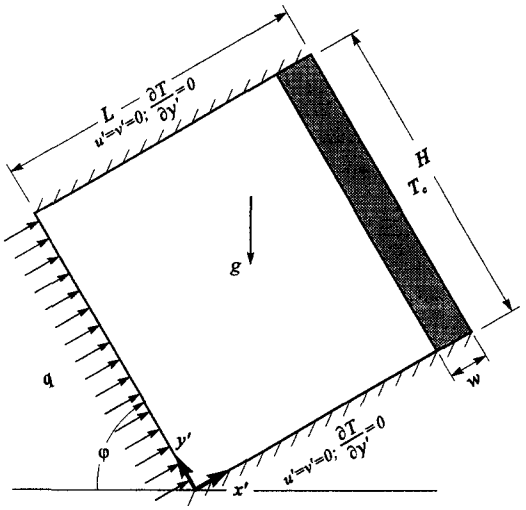

Fig. 1. Problem geometry and boundary conditions.

MATHEMATICAL MODELLING

The following non-dimensional variables are defined

$$x = \frac{x^*}{L} \quad y = \frac{y^*}{L} \quad u = \frac{u^* L}{\alpha} \quad v = \frac{v^* L}{\alpha}$$

Table 1. Empirical constants used in the turbulence model

C_1	C_2	C_μ	σ_k	σ_ε	Pr_t	χ	E
1.45	1.95	0.09	1.00	1.30	1.00	0.41	9.00

$$p = \frac{p^* + \rho g(x^* \cos\varphi + y^* \sin\varphi) + \frac{2}{3}\rho\kappa^*}{\rho(\alpha/L)^2} \quad \theta = \frac{T - T_o}{Lq/k_f}$$

$$\kappa = \frac{\kappa^* L^2}{\alpha^2} \quad \varepsilon = \frac{\varepsilon^* L^4}{\alpha^3} \quad t = \frac{\alpha}{L^2} t^*. \tag{1}$$

The non-dimensional form of the governing equations are obtained as follows (incompressible flow and Boussinesq approximation):

$$\frac{\partial u}{\partial x} + \frac{\partial v}{\partial y} = 0 \tag{2}$$

$$\frac{\partial u}{\partial t} + u\frac{\partial u}{\partial x} + v\frac{\partial u}{\partial y} = -\frac{\partial p}{\partial x} + \lambda Pr\nabla^2(\mu_e u) + RaPr\theta\cos\varphi + S_u \tag{3}$$

$$\frac{\partial v}{\partial t} + u\frac{\partial v}{\partial x} + v\frac{\partial v}{\partial y} = -\frac{\partial p}{\partial y} + \lambda Pr\nabla^2(\mu_e v) + RaPr\theta\sin\varphi + S_v \tag{4}$$

$$\frac{\partial \theta}{\partial t} + u\frac{\partial \theta}{\partial x} + v\frac{\partial \theta}{\partial y} = k_r\nabla^2(\alpha_e\theta) \tag{5}$$

$$\frac{\partial \kappa}{\partial t} + u\frac{\partial \kappa}{\partial x} + v\frac{\partial \kappa}{\partial y} = Pr\nabla^2\left(\frac{\mu_e}{\sigma_\kappa}\kappa\right) + S_\kappa \tag{6}$$

$$\frac{\partial \varepsilon}{\partial t} + u\frac{\partial \varepsilon}{\partial x} + v\frac{\partial \varepsilon}{\partial y} = Pr\nabla^2\left(\frac{\mu_e}{\sigma_\varepsilon}\varepsilon\right) + S_\varepsilon \tag{7}$$

where μ_e and α_e are defined as

$$\mu_e = 1 + \mu_t = 1 + c_\mu\frac{\kappa^2}{Pr\varepsilon} \quad \alpha_e = 1 + \alpha_t = 1 + \mu_t\frac{Pr}{Pr_t}. \tag{8}$$

λ and k_r in equations (3)–(5) are both equal to 1 in the fluid region, and to 10^{15} and k_w/k_f, respectively, in the solid region.

The problem is governed by non-dimensional parameters of Ra, Pr, which are defined as

$$Ra = \frac{g\beta q L^4}{\nu\alpha k_f} \quad Pr = \frac{\nu}{\alpha}. \tag{9}$$

The boundary conditions are the no-slip conditions on all the rigid wall surfaces, isothermal temperature on the outer surface of the wall, constant heat flux on the side opposing the wall and adiabatic on the horizontal walls. Hence, the boundary conditions for this problem are as shown in Fig. 1.

In the near wall regions, steep nonlinear gradients and relatively low level of turbulence exist. To account for these, the wall function method is used [10]. Thus in the near wall region of the flow, where $\delta^+ > 12$, the constant shear stress is calculated using the log-law

$$\frac{u_p}{u_\tau} = \frac{1}{\chi}\ln\left(\frac{E\delta u_\tau}{Pr}\right) \quad \delta^+ = \frac{\delta u_\tau}{Pr}. \tag{10}$$

For $\delta^+ < 12$, the laminar shear stress relation is used

$$u_\tau = \sqrt{\frac{Pr\, u_p}{\delta}}. \tag{11}$$

The recommended empirical constants used in the present model are summarized in Table 1 [12].

The law of the wall is incorporated in equations (3) and (4), where the convection terms are neglected and an effective viscosity is assumed according to equation (8) and

$$\kappa_p = \frac{u_\tau^2}{\sqrt{c_\mu}} \quad \varepsilon_p = \frac{u_\tau^3}{\chi\delta}. \tag{12}$$

The same formulation applies also to the energy equation in the near wall region where the temperature profile is described in terms of a wall function.

The stream function is calculated from its definition

$$u = -\frac{\partial \psi}{\partial y} \quad v = \frac{\partial \psi}{\partial x} \tag{13}$$

and by assuming $\psi = 0$ at the boundaries.

VALIDATION OF THE CODE AND COMPUTATION

The numerical method used to solve the system of equations (2)–(7) is the SIMPLER method [13]. The computer code based on the mathematical model above is validated for various cases. The results and the deviations from the bench mark solutions [14] are summarized in Table 2. The comparison was also made with the results of Le Breton *et al.* [15] who used the same solution technique as in this study. The maximum deviations of the same parameters, i.e. ψ_{max}, U_{max}, V_{max} and Nu_o (the average Nusselt number along the vertical wall [14]), were 2.3, 1.4, 0.7 and 1.1%, respectively. A nonuniform grid size in both directions was used in this study with a minimum five control volumes in solid media in the x direction. The code with a nonuniform grid produced results, which compared a little better with the bench mark solutions.

The code was also validated by solving the problem of a square cavity for $Ra = 10^{10}$. A comparison with Markatos and Pericleous [4] for the case of a square cavity showed that the agreement for various parameters was within $\pm 10\%$. Comparisons with the works by Henkes *et al.* [6], and Abadie and Schiestel [8] showed qualitative agreement.

Independence of solution on the grid size was studied

Table 2. Results for $Ra = 1 \times 10^6$ with grid size of 42×42, regular and irregular mesh

	Bench mark [14]	De Vahl Davis [14]	This study			
			Regular mesh	Error [%]	Irregular mesh	Error [%]
ψ_{max}	16.75	17.613	17.531	4.66	17.025	1.64
(x, y)	0.151, 0.547	0.151, 0.542	0.15, 0.55	0.66, 0.55	0.164, 0.547	
U_{max}	64.63	67.49	66.79	3.34	65.47	1.30
y	0.85	0.854	0.863	1.53	0.880	
V_{max}	219.36	206.32	223.49	1.88	221.09	0.79
x	0.0379	0.0423	0.038	0.26	0.041	
Nu_0	8.817	9.270	9.417	6.81	8.735	0.93

for various cases, k_r and W. For instance, for $Ra = 10^{12}$, $\varphi = 90°$, $k_r = 10$, $w = 0.15$, the grid sizes of 42×32, 42×42, 62×52 and 82×72 were tried. The results showed that grid independence was achieved above 42×42, showing acceptable differences in heat transfer (0.47%) and ψ_{max} (3.76%). For smaller aspect ratios, the grid independence was ensured using 42×32 grid size. In any case, the Nusselt numbers for various k_r showed similar trends as a function of grid size, ensuring the observed conclusion of grid independence. The results for $A = 1$ presented in this study were with 42×42 grid size; for smaller aspect ratios, it was with 42×32. Grid refinement near the boundary was used to reduce the computing time.

To control the convergence better, steady solutions were obtained from transient equations. The time step Δt was varied from 10^{-4} for low Rayleigh numbers to 10^{-5} for high Rayleigh numbers. The relaxation coefficient was maintained at 0.7. For instance, for $Ra = 10^{10}$, $W = 0.15$, $\varphi = 90°$, $k_r = 10$, using 42×42 grid size, the solution was obtained after 4000 iterations requiring about 3 h on an IBM RS/6000-365 work station.

The convergence criterion was based on the corrected pressure field. When the correction terms were small enough so that no difference existed between the pressure field before and after correction, iterations were advanced in time until

$$\Sigma|\Phi_{i,j}^{t+\Delta t} - \Phi_{i,j}^{t}| < 10^{-4} \tag{14}$$

where Φ stands for u, v and θ.

In addition to the usual accuracy control, the accuracy of computations was controlled using the energy conservation within the system.

RESULTS AND DISCUSSION

Flow and temperature fields and heat transfer rates are examined for ranges of the Rayleigh number and geometrical parameters of the problem. In the present study, the following geometrical configurations were taken as base: $\varphi = 90°$ corresponding to vertical configuration, $A = 1$ (square enclosure), dimensionless wall thickness, $W = 0.15$, conductivity ratio, $k_r = 10$, $Pr = 0.72$ (air). Effects of the dimensionless wall thickness W and conductivity ratio k_r were studied by varying them from 0 to 0.50 and from 1 to 10, respectively. The range of the Rayleigh number, characterizing the natural convection, was from 10^8 to 10^{12}. The effects of the enclosure aspect ratio, A, and of the inclination, φ, were also examined by varying them from 1 to 0.5 and from 0 to 180°, respectively.

General observations

The streamlines and isotherms in the domain of computation for $k_r = 10$, $W = 0.15$, $\varphi = 90°$ and Ra from 10^8 to 10^{12} are shown in Fig. 2(a)–(c), and those for $Ra = 10^{11}$, $W = 0.15$ and k_r from 1 to 10 in Fig. 3(a)–(c), respectively. The effect of the dimensionless wall thickness is shown in Fig. 4(a) and (b) and Fig. 3(c).

The results in Fig. 2 are with $k_r = 10$, which correspond to the case with relatively high wall conductivity. Hence, for $Ra = 10^8$, the temperature gradient within the solid wall is very small and the temperature at the internal surface is almost the same as the imposed uniform temperature at its outer boundary. For $Ra > 10^8$, the isotherms show a considerable temperature gradient in the wall. For increasing Ra, the isotherms show a stratified flow within the enclosure with steep gradients near the vertical boundaries. It is seen that, near the left boundary and at the inner surface of the wall, a thermal boundary layer is formed. The streamlines in Fig. 2 show increasing convection with increasing Ra. For all Ra, the streamlines are quasi-symmetric, except for $Ra = 10^8$ for which they are a little skewed with increasing flow near the vertical boundaries and $|\psi_{max}|$ is displaced towards the massive wall, at $x = 0.755$, $y = 0.5$. For increasing Ra, $|\psi_{max}|$ displaces to $x = 0.803$, $y = 0.5$ for $Ra = 10^{10}$ and $x = 0.830$, $y = 0.55$ for $Ra = 10^{12}$.

The effect of the conductivity ratio, k_r, on the heat transfer is shown in Fig. 3(a)–(c) for $Ra = 10^{11}$ and $W = 0.15$. Although there is no discernible difference in streamlines when k_r is varied from 1 to 10, while keeping the other parameters the same, $|\psi_{max}|$ show that the convection has increased with increasing k_r. $|\psi_{max}|$ values are 34.623, 50.231 and 63.630 for $k_r = 1$, 5 and 10, respectively, with their positions remaining the same. Similar results for $Ra = 10^{12}$ (not shown here) showed that the position of $|\psi_{max}|$ was displaced considerably towards the lower part of the massive wall. These results are expected since the temperature of the inner surface of the wall increases with increas-

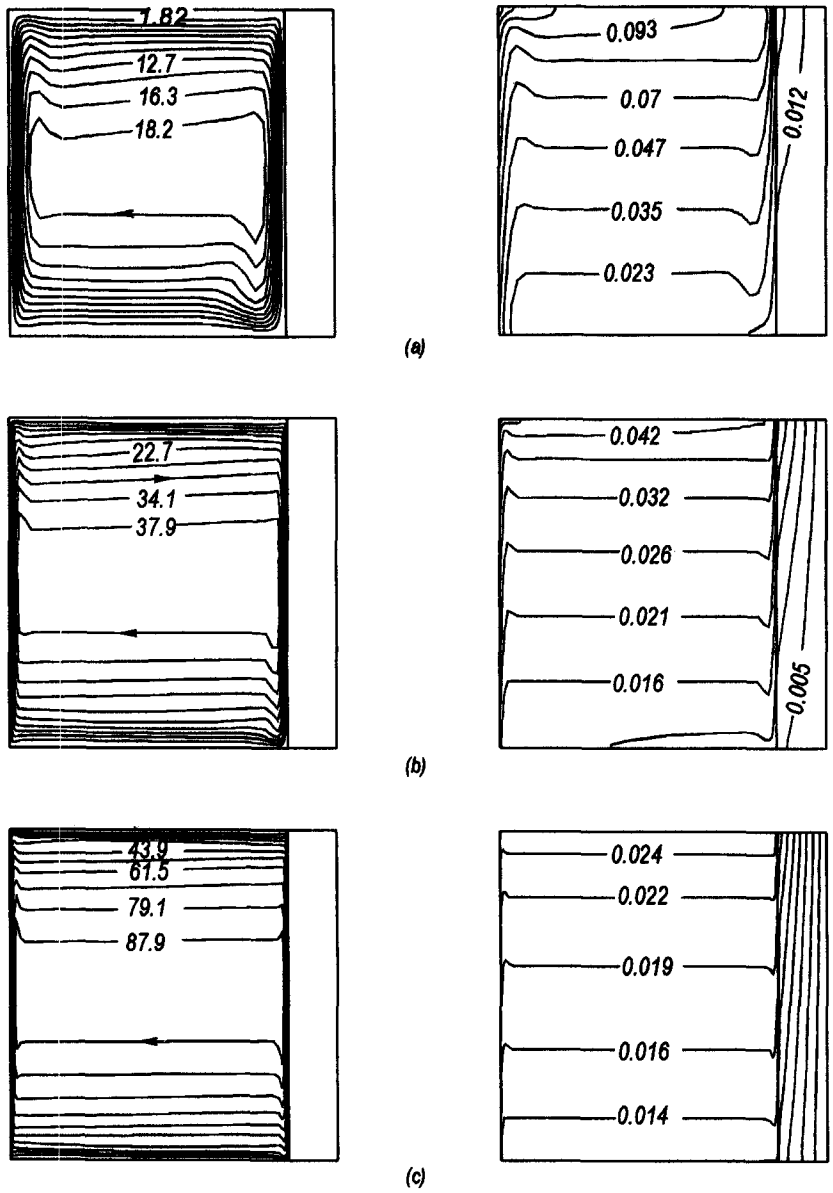

Fig. 2. Streamlines (on the left) and isotherms (on the right) in enclosure with $A = 1$ and $\varphi = 90°$, $k_r = 10$, $W = 0.15$ and various Rayleigh numbers. (a) $Ra = 10^8$, $\psi_{max} = 19.98(0.755, 0.5)$, (b) $Ra = 10^{10}$, $\psi_{max} = 41.73(0.803, 0.5)$ and (c) $Ra = 10^{12}$, $\psi_{max} = 96.70(0.83, 0.5)$.

ing k_r, which can be confirmed by examining the isotherms. The results show a large temperature gradient for $k_r = 1$ in Fig. 3(a), that becomes negligibly small as k_r increases as in Fig. 3(b) and (c). As a result, the convection increases since the temperature differential becomes larger with increasing k_r, supporting the observation made with the streamlines.

Figures 4 and 3(c) show the effect of the dimensionless wall thickness on the flow and temperature fields for $Ra = 10^{11}$ and $k_r = 10$. The enclosure becomes more rectangular as W increases and the strength of the convection is altered. For $k_r = 10$, the temperature gradient is small for $W = 0.15$: it increases with increasing wall thickness, thus affecting the inner surface temperature of the wall. As a result, the convection increases. In fact, $|\psi_{max}|$ are 63.630 for $W = 0.15$, 62.023 for $W = 0.3$ and 49.652 for $W = 0.5$ and their position at the center of the enclosure is displaced slightly upward with increasing W.

Heat transfer

Heat transfer as a function of various parameters is evaluated and presented as the normalized Nusselt number as a function of dimensionless parameters in Figs. 5 and 6. The normalized Nusselt number as a function of the Rayleigh number with W and k_r as

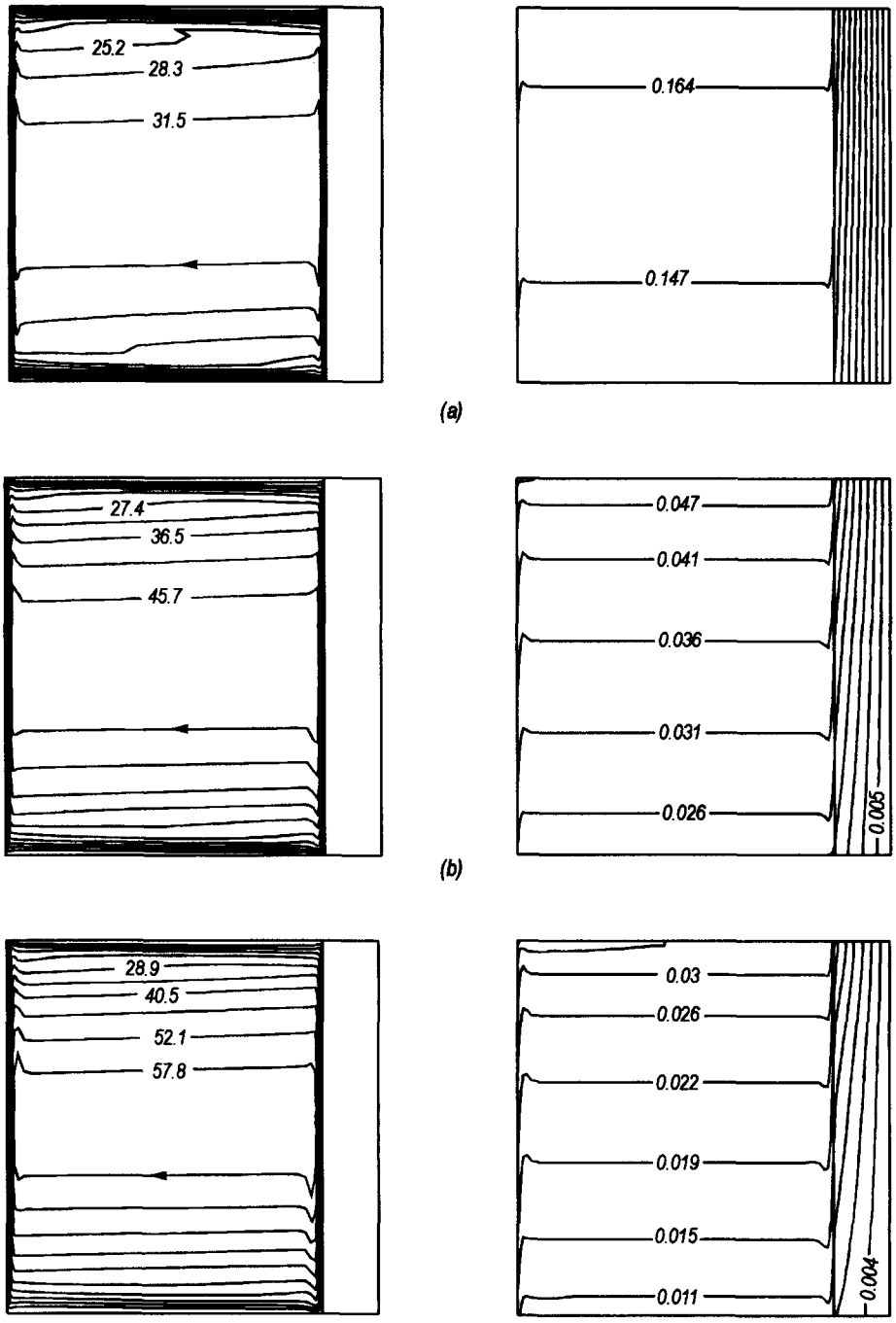

Fig. 3. Streamlines (on the left) and isotherms (on the right) in enclosure with $A = 1$ and $\varphi = 90°$, $Ra = 10^{11}$, $W = 0.15$ and various conductivities. (a) $k_r = 1$, $\psi_{max} = 34.62(0.83, 0.5)$, (b) $k_r = 5$, $\psi_{max} = 50.23(0.819, 0.5)$ and (c) $k_r = 10$, $\psi_{max} = 63.63(0.819, 0.5)$.

parameters is shown in Fig. 5. Heat transfer increases with increasing Rayleigh number, with decreasing wall thickness and with increasing wall conductivity. As observed earlier with Figs. 2 and 3, it is seen that, for $k_r = 1$, the heat transfer is only little affected by the Rayleigh number. For increasing k_r, the convection becomes important and the heat transfer is a strong function of Ra. With increasing wall thickness, it is seen that heat transfer by conduction becomes considerable as was the case observed in Fig. 4.

The effect of wall conductivity on the heat transfer is shown in Fig. 6. It is seen that Nu is an increasing function of k_r, weak at low Ra and strong at high Ra with the same trend for different wall thicknesses. The

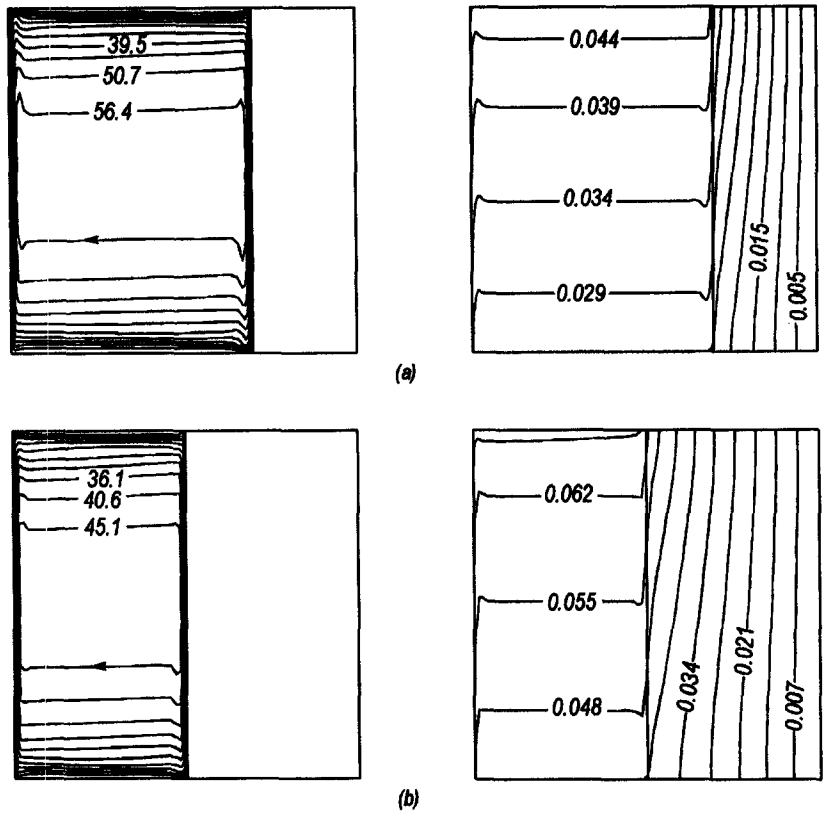

Fig. 4. Streamlines (on the left) and isotherms (on the right) in enclosure with $A = 1$ and $\varphi = 90°$, $Ra = 10^{11}$, $k_r = 10$ and various wall thicknesses. (a) $W = 0.3$, $\psi_{max} = 62.02(0.669, 0.5)$ and (b) $W = 0.5$, $\psi_{max} = 49.65(0.469, 0.5)$.

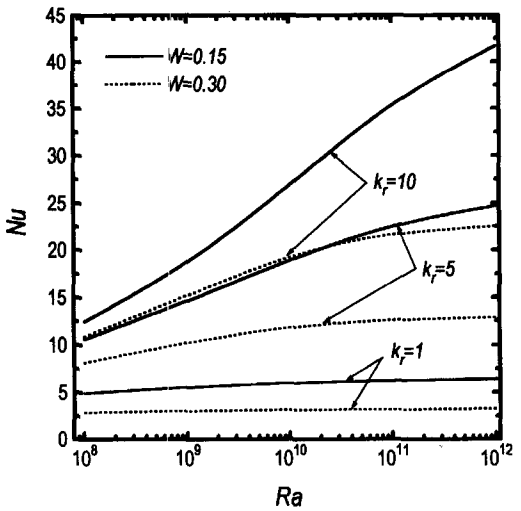

Fig. 5. Normalized Nusselt number as a function of the Rayleigh number for various wall thicknesses and conductivities.

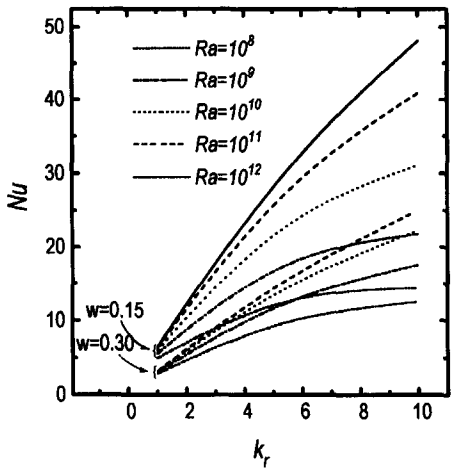

Fig. 6. Normalized Nusselt number as a function of the wall conductivity for various Rayleigh numbers and wall thicknesses.

reason is due to the fact that convection is not affected beyond a wall conductivity as the wall inner surface temperature becomes almost the same as that of the wall outer surface. This was observed in Figs. 2 and 3. In fact, for $k_r \geqslant 5$ and, at low Rayleigh numbers, there is only a small temperature gradient in the massive wall, and, as a result, the variation of Nu is less sensitive to k_r. It should be noted that the dimensionless conductivities for various construction materials are usually between 1 and 10, for well insulated partitions and walls having $k_r \approx 1$.

Table 3. Nu, ψ_{max}, $\psi_{max}/\Delta y$ for various A, k_r and Ra

		$k_r = 5$			$K_r = 10$		
	A	Nu	ψ_{max}	$\psi_{max}/\Delta y$	Nu	ψ_{max}	$\psi_{max}/\Delta y$
$Ra = 10^{10}$	0.5	21.512	24.354	88.239	31.523	27.615	110.460
	1.0	21.376	36.132	72.264	30.866	43.011	86.022
$Ra = 10^{11}$	0.5	25.649	34.222	123.993	41.473	39.794	144.181
	1.0	25.589	50.231	100.462	40.922	63.630	127.260

Effect of aspect ratio

The effect of the aspect ratio on the heat transfer is studied for the case of $Ra = 10^{10}$ and 10^{11}, $W = 0.15$ and $k_r = 1, 5, 10$. The aspect ratio, A, was varied from 0.5 to 1.0 with the former value corresponding to a rectangular enclosure twice the height, simulating an elongated enclosure. The results are presented in Fig. 7 as Nu vs A. Generally, Nu increases with increasing k_r at any A. This is expected in view of the earlier observation made for Figs. 5 and 6. For $Ra = 10^{10}$ and 10^{11}, Fig. 7 shows that Nu is a slightly decreasing function of A for all k_r although less discernible for $k_r = 1$. To explain this phenomenon, flow fields in various cases were examined. ψ_{max} values for $Ra = 10^{10}$, 10^{11} and $k_r = 5$, 10 are presented in Table 3. Normally, Nu should be an increasing function of ψ_{max}, since it is known that the natural convection increases with increasing strength of circulation, ψ_{max}. The reason for the observed phenomenon is in fact due to a decreased flow rate. From the scale analysis of laminar natural convection in enclosures, it is known that $u \sim (\alpha/H)\, Ra_H^{1/2}$, $Nu \sim Ra_H^{1/4}$; therefore, $Nu \sim u^{1/2}$ [16]. $\psi_{max}/\Delta y$ being proportional to the average flow rate or the average velocity, $Nu \sim$ (gradient of $\psi)^{1/2}$. $(\psi_{max} - \psi_{y=0})/\Delta y = \psi_{max}/\Delta y$ are calculated and shown in Table 3. It is seen that $\psi_{max}/\Delta y$ is a decreasing function of A despite the fact that ψ_{max} is an increasing function of it. The results show that this phenomenon is observed easier when k_r is high as for $k_r = 5$ and 10. For high k_r, the wall becomes more conductive and the temperature at the inner surface of the wall becomes identical to that at its outer surface. For this case, the heat transfer phenomenon resembles that in an enclosure with two sides without thermal resistance. It is known for the laminar case in such enclosures that Nu is a decreasing function of the aspect ratio when the aspect ratio has an order of magnitude of 1. Also, as is the case here, the variation is Ra dependent [16].

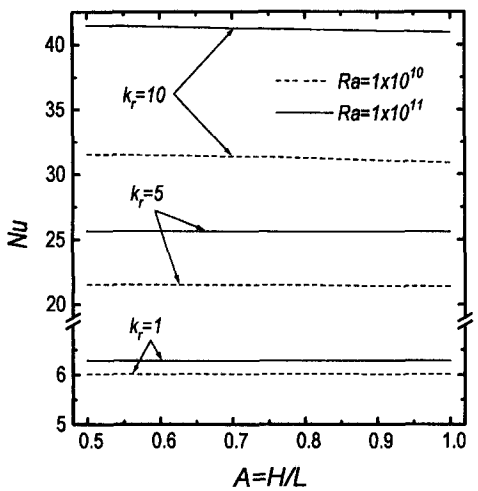

Fig. 7. Normalized Nusselt number as function of the enclosure aspect ratio for $Ra = 10^{10}$ and 10^{11}, $W = 0.15$ and $k_r = 1, 5, 10$.

Effect of inclination

The effect of the inclination angle is studied by varying φ from 0 to 180°. The case of $Ra = 10^{10}$, $W = 0.15$, $k_r = 10$, and $A = 0.5$ and 1 is presented in Figs. 8–11. Flow and temperature fields for $A = 1$ and $\varphi = 30$, 45, 60, 75, 150° are shown in Fig. 8(a)–(e), and similar results for $A = 0.5$, $\varphi = 30$, 60, 120, 150° are shown in Fig. 9. The heat transfer, Nu, as function of the inclination angle, φ, and for two aspect ratios is presented in Fig. 10. Nu_{loc} along the side opposing the wall as a function of φ is shown in Fig. 11.

The effect of φ on the flow field in a square enclosure at various angles is seen in Fig. 8(a)–(e), where the position of the enclosure for each inclination is shown in the middle, and Fig. 2(b) for $\varphi = 90°$. It is noted that $\varphi = 0$ corresponds to the case where the heat flux is from the bottom and 180° from the top (pure conduction). Starting from the horizontal case, streamlines are deformed in the direction of gravity and as the wall with constant heat flux becomes positioned at the top, the heat transfer becomes more dominated by conduction. Isotherms on the right-hand side clearly show this situation. Isotherms for $\varphi = 150°$, for instance, show a dominant conduction regime. $|\psi_{max}|$ for increasing φ from 30 to 150° in Fig. 8 were 237.826, 169.139, 109.633, 68.133, 12.155, showing the same trend.

Similar results for $A = 0.5$ are presented in Fig. 9(a)–(d). It is seen that, for $\varphi \geqslant 90°$, the heat transfer becomes dominated by conduction and the flow field is confined to almost half of the enclosure adjacent to the right wall. $|\psi_{max}|$ for increasing φ from 30 to 150° in Fig. 9 were 164.873, 131.383, 10.941, 7.754, respectively. Comparison of Figs. 8 and 9 shows that, for the same inclination angle, the strength of convection is reduced when the enclosure is elongated.

Heat transfer as a function of inclination angle for two aspect ratios presented in Fig. 10 is seen to produce the observations made in Figs. 8 and 9. $Nu = 1$

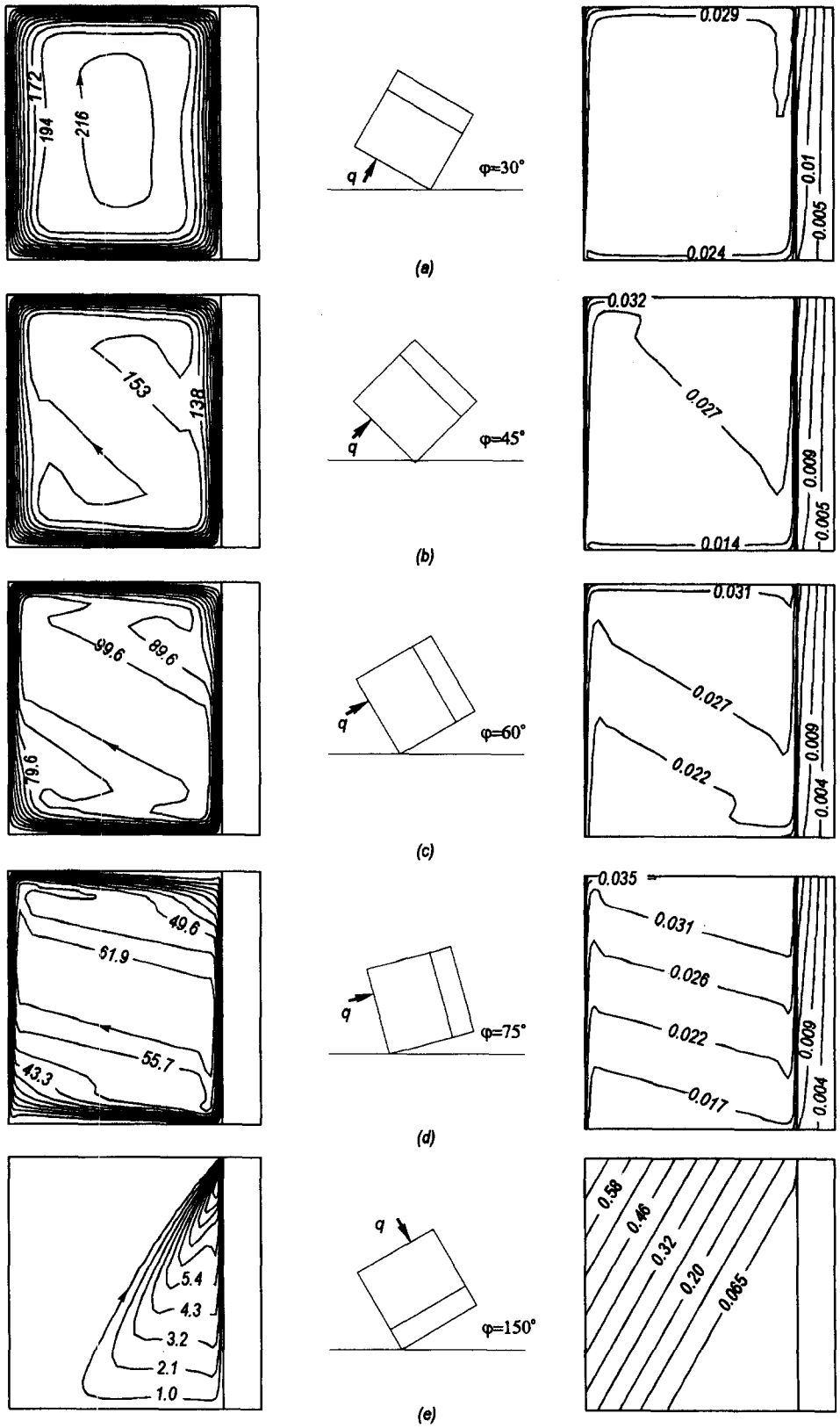

Fig. 8. Streamlines (on the left) and isotherms (on the right) in enclosures with $A = 1$, $k_r = 10$, $W = 0.15$, $Ra = 10^{10}$ and various inclination angles. (a) $\varphi = 30°$; $\psi_{max} = 237.82(0.211, 0.211)$, (b) $\varphi = 45°$; $\psi_{max} = 169.14(0.683, 0.11)$, (c) $\varphi = 60°$; $\psi_{max} = 109.63(0.095, 0.915)$, (d) $\varphi = 75°$; $\psi_{max} = 68.13(0.803, 0.401)$ and (e) $\varphi = 150°$; $\psi_{max} = 12.15(0.83, 0.889)$.

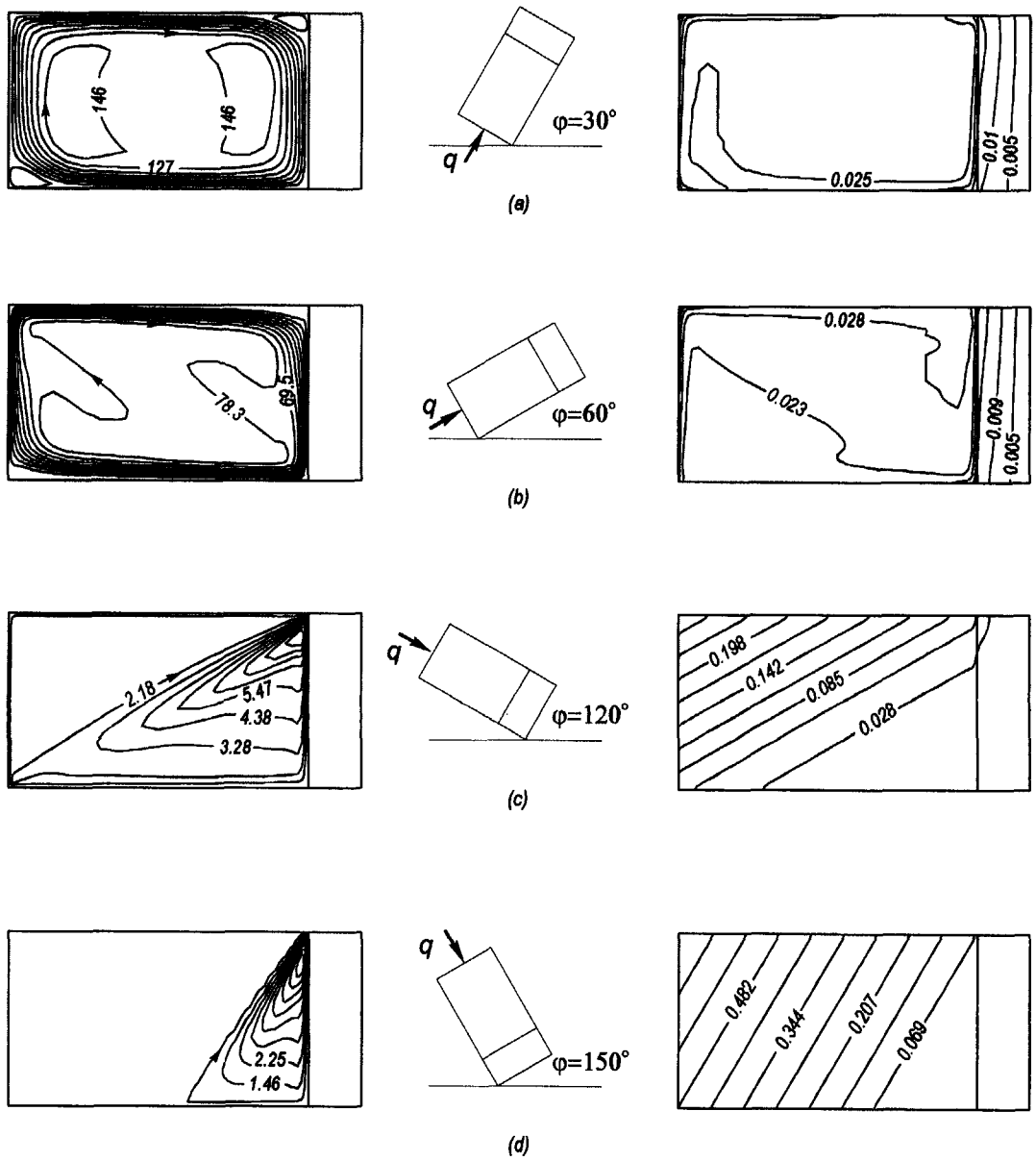

Fig. 9. Streamlines (on the left) and isotherms (on the right) in enclosures with $A = 0.5$, $k_r = 10$, $W = 0.15$, $Ra = 10^{10}$ and various inclination angles. (a) $\varphi = 30°$; $\psi_{max} = 164.87(0.167, 0.173)$, (b) $\varphi = 60°$; $\psi_{max} = 87.08(0.167, 0.127)$, (c) $\varphi = 120°$; $\psi_{max} = 10.94(0.83, 0.428)$ and (d) $\varphi = 150°$; $\psi_{max} = 7.75(0.83, 0.411)$.

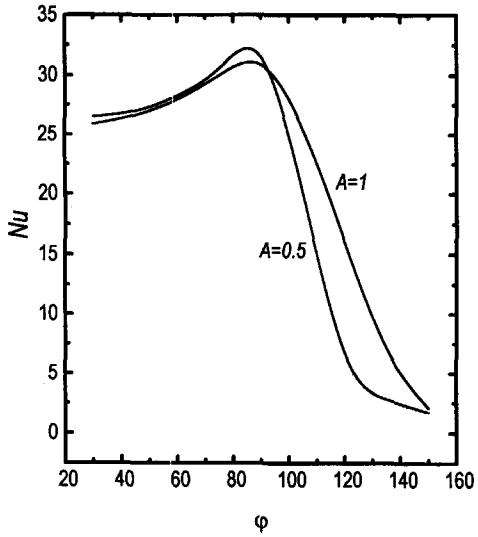

Fig. 10. Normalized Nusselt number as a function of the enclosure inclination angle for $Ra = 10^{10}$, $W = 0.15$, $k_r = 10$ and $A = 0.5, 1$.

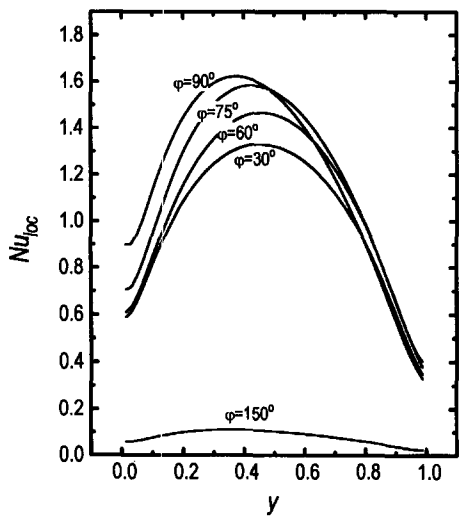

Fig. 11. Local Nusselt number along the left wall for various inclination angles. $Ra = 10^{10}$, $W = 0.15$, $k_r = 10$ and $A = 1$.

for $\varphi = 180°$ (conduction regime) and it increases with decreasing inclination, as the heat transfer becomes dominated by natural convection. Nu passes from a maximum for $80° < \varphi < 90°$, an observation made also for the laminar case with a square cavity without a bounding wall [17] and with a bounding wall [3]. It is seen that, for $\varphi > 90°$, the convection is less violent in elongated enclosures, as observed in Figs. 8 and 9.

Nu_{loc} along the left wall for various inclination angles is shown in Fig. 11 for the case of $Ra = 10^{10}$, $A = 1$ and $k_r = 10$. Generally, Nu_{loc} is an increasing function of φ, when it is varied from 30 to 90°, and it is dominated by the conduction regime when $\varphi > 120°$. It is observed that Nu_{loc} passes from a maximum, the extremum of which shifting to lower y for increasing inclination angle, obviously due to shifting gravity direction in the enclosure.

It should be noted that, in turbulent flow, at any inclination angle smaller than $\varphi = 90°$ the flow is distorted whereas in laminar flow this was noticed only at angles near 60° [3]. Also, the dependency of Nu on the aspect ratio is less evident in turbulent flow than in laminar and it appears that the heat transfer rate decreases with A. Similar trends are found in laminar flow for this range of A considered in this study [16].

Heat transfer correlation

Heat transfer correlations, Nu as a function of the Rayleigh number, Ra, the aspect ratio, A, conductivity ratio, k_r, wall thickness, W and inclination angle, φ, were derived based on functional forms

$$Nu_{\varphi=90} = aRa^b A^c k_r^d W^e \tag{15}$$

$$Nu_{\varphi} = Nu_{\varphi=90}(\sin\varphi)^f \tag{16}$$

where the coefficients a to f are determined by using a least square technique as $a = 0.1307$, $b = 0.1$, $c = -1/9$, $d = 0.75$, $e = -0.75$; $f = -0.01$ for $0° \leqslant \varphi \leqslant 90°$ and $f = 6.0$ for $90° < \varphi \leqslant 180°$.

The limits of the correlation are $10^8 \leqslant Ra \leqslant 10^{12}$, $0.5 \leqslant A \leqslant 1$, $1 \leqslant k_r \leqslant 10$, $0 \leqslant W \leqslant 0.5$ and $0° \leqslant \varphi \leqslant 180°$. The correlation coefficient, R, was 0.9754 for equation (15) and 0.9524 for $0 \leqslant \varphi \leqslant 90°$ and 0.9554 for $90° < \varphi \leqslant 180°$ in equation (16).

The correlations with equation (16) for the two regions of φ are presented in Fig. 12(a) and (b). It is seen that the effect of Ra is negligible, particularly for low k_r and high W as is evident from Figs. 5 and 6. As expected, the effects of k_r and W are similar and inverse. As equation (16) shows, the effect of the inclination angle, φ, is different for the two regions. It is noted that, for many applications in the building industry and passive solar energy utilization, $60° \leqslant \varphi \leqslant 120°$.

Remarks on turbulence

The flow is mainly divided into two principal regions: a region where the fluid is stagnant and stratified in the core, and the other near the heated and cooled walls where the effective viscosity is larger then unity and a boundary layer type of flow is developed. The boundary layer type of flow is shown in Fig. 13 for $Ra = 10^{12}$. It is seen that the velocity gradient near the wall is very high. The boundary layer develops early near the bottom of the heated side and reaches a maximum at about half the height of the cavity. Evidently, the boundary layer cannot be completely turbulent since it is observed in Fig. 14 that isolines of the turbulent viscosity show that μ_t is more important in the second half of the cavity. This suggests that a critical distance y_{tr} exists beyond which the flow is turbulent [18]. The flow is re-laminarized at the end of the vertical wall to join the horizontal stream parallel to the adiabatic plane. The transition from laminar to turbulent regime at the bottom of the

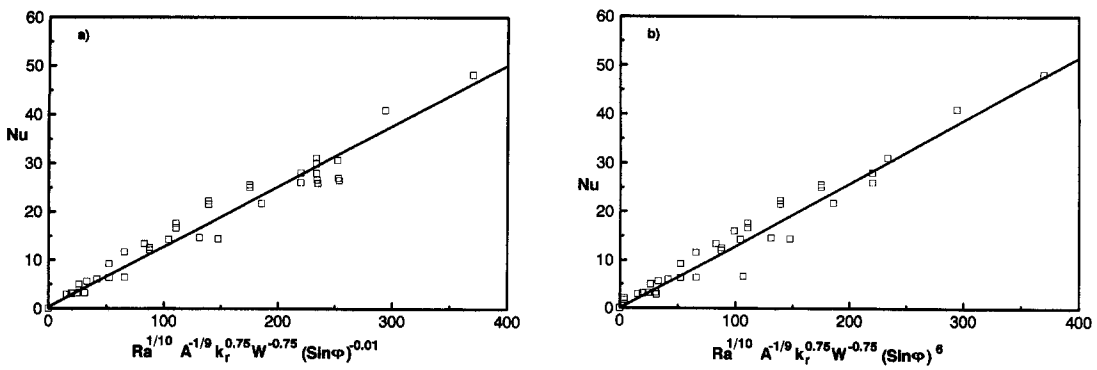

Fig. 12. Heat transfer correlation Nu as a function of the group $Ra^{0.1}A^{-1/9}k_r^{0.75}W^{-0.75}\sin\varphi^f$. (a) $0° \leqslant \varphi \leqslant 90°$ with $f = -0.01$, (b) $90 < \varphi \leqslant 180°$ with $f = 6$.

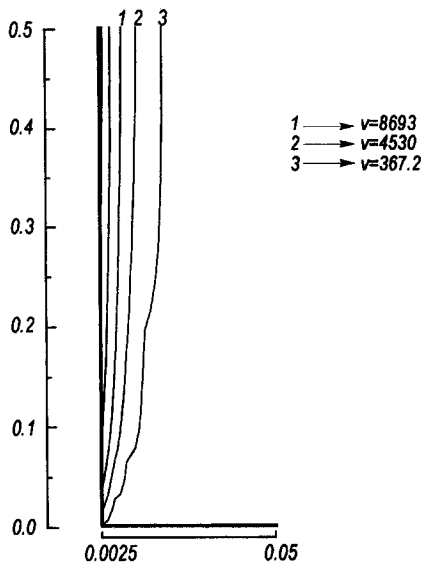

Fig. 13. Boundary layer on the heated side for $Ra = 10^{10}$.

heated wall is not clearly defined, as was also observed for the case of a differentially heated enclosure [6].

Figure 15 shows direct relationships between $\sqrt{\kappa}$ and Ra, and μ_t and Ra near the heated wall. Both μ_t and κ have similar behaviour with increasing Ra. For $Ra = 10^{12}$, the dissipation rate of the turbulent energy becomes important near the walls, as μ_t is influenced by κ:

$$\mu_t = c_\mu \frac{\kappa^2}{\varepsilon}. \tag{17}$$

CONCLUSIONS

Turbulent natural convection in enclosures bounded by a solid wall has been studied. Two-dimensional equations of conservation of mass, momentum and energy, with the Boussinesq approximation, have been solved using a finite difference method. The κ–ε model is used for turbulence. Governing parameters were $10^8 \leqslant Ra \leqslant 10^{12}$, $1 \leqslant k_r \leqslant 10$, $0 \leqslant W \leqslant 0.5$, $0.5 \leqslant$

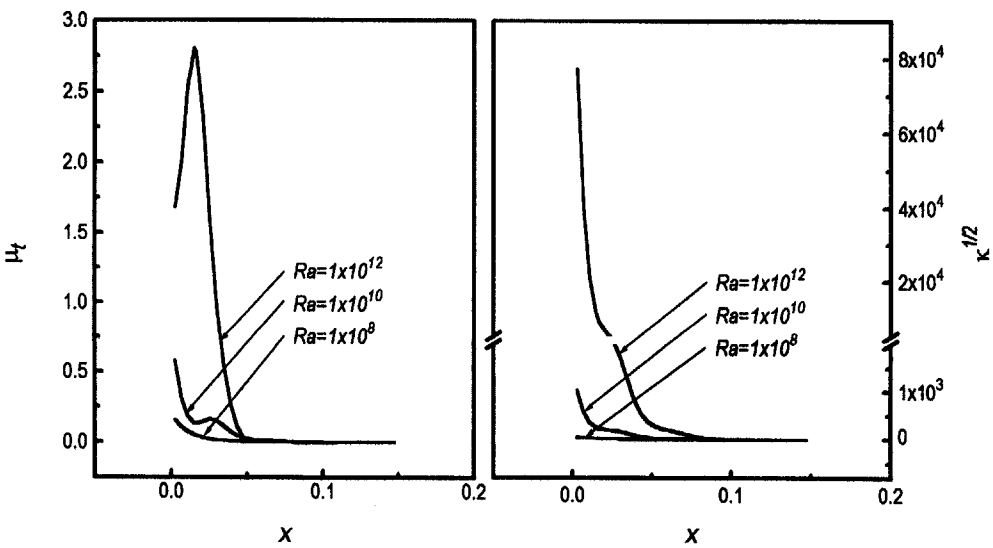

Fig. 14. Isolines of turbulent viscosity for (a) $Ra = 10^{10}$, (b) $Ra = 10^{12}$.

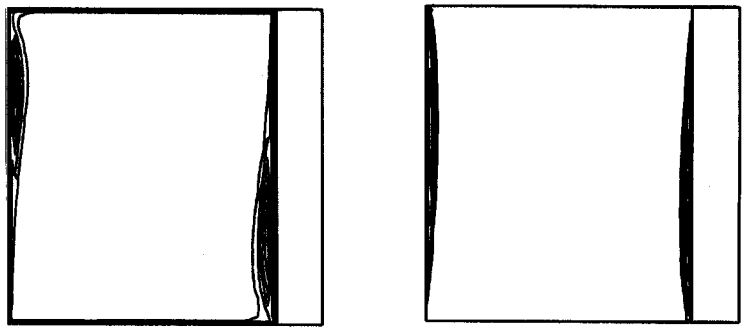

Fig. 15. Profiles of turbulent viscosity and of kinetic energy of turbulence near the heated side of the cavity for various Rayleigh numbers.

$A \leqslant 1$ and $0 \leqslant \varphi \leqslant 180°$. The results showed that (1) heat transfer is an increasing function of the Rayleigh number and of the wall conductivity ratio (it is a weak function of the enclosure aspect ratio); (2) it is a decreasing function of the wall thickness; (3) heat transfer has a maximum for an inclination angle of 80–90° and (4) these trends are amplified at high Rayleigh numbers, at high wall conductivity and at small wall thickness.

Acknowledgements—Financial support by the Natural Sciences and Engineering Research Council of Canada is acknowledged. We like to thank Mr. Amavi Kangni who carried out some computations and heat transfer correlation study.

REFERENCES

1. I. Catton, Natural convection in enclosures, *Proceedings of the Sixth International Heat Transfer Conference*, Vol. 6, pp. 13–31 (1978).
2. B. Gebhart, Y. Jaluria, R. P. Mahajan and B. Sammakia, *Buoyancy-Induced Flows and Transport*. Hemisphere, New York (1988).
3. R. Ben Yedder and E. Bilgen, Heat transfer by natural convection and conduction in enclosures bounded by a solid wall, *Numer. Meth. Heat. Fluid Flow* (submitted).
4. N. C. Markatos and K. A. Pericleous, Laminar and turbulent natural convection in an enclosed cavity, *Int. J. Heat Mass Transfer* **27**, 755–772 (1984).
5. C. P. Thompson, N. S. Wilkes and I. P. Jones, Numerical studies of buoyancy-driven turbulent flow in a rectangular cavity, *Int. J. Numer. Meth. Engng* **24**, 89–99 (1987).
6. R. A. W. M. Henkes, F. F. Van Der Vlugt and C. J. Hoogendoorn, Natural convection flow in a square cavity calculated with low-Reynolds-number turbulence models, *Int. J. Heat Mass Transfer* **34**(2), 377–388 (1991).
7. C. Nonino and S. Del Giudice, Turbulent forced convection in two-dimensional recirculating flows, *Numer. Meth. Thermal Problems*, pp. 332–344 (1985).
8. P. Abadie et R. Schiestel, Prévision numérique de la convection forcée dans une cavité bidimensionnelle entraînée, *Int. J. Heat Mass Transfer* **29**(3), 417–427 (1986).
9. M. Nallasamy, Turbulence models and their applications to the predictions of internal flows: a review, *Comput. Fluids* **15**, 151–194 (1987).
10. W. Rodi, *Turbulence Models and Their Applications in Hydraulics*. International Association for Hydraulic Research, Delft, The Netherlands (1980).
11. C. Begheim, F. Penot, S. Mergui and F. Allard, Numerical and experimental evaluation of turbulent models for natural convection simulation in a thermally driven square cavity, Proc. of the ASME Winter Annual Meeting, Paper 93-WA/HT-46 (1993).
12. B. E. Launder and D. B. Spalding, The numerical computation of turbulent flows, *Comp. Meth. Appl. Mech. Engng* **3**, 269–289 (1974).
13. S. V. Patankar, *Numerical Heat Transfer and Fluid Flow*. Hemisphere, Washington, DC (1980).
14. G. De Vahl Davis and I. P. Jones, Natural convection in a square cavity: a comparison exercise, *Int. J. Numer. Meth. Fluids* **3**, 227–248 (1983).
15. P. Le Breton, J. P. Caltagirone and E. Arquis, Natural convection in a square cavity with thin porous layers on its vertical walls, *J. Heat Transfer* **113**, 892–898 (1991).
16. A. Bejan, *Convection Heat Transfer*. Wiley, New York (1985).
17. R. A. Kuyper, Th. H. van der Meer, C. J. Hoogendoorn and R. A. W. M. Henkes, Numerical study of laminar and turbulent natural convection in an inclined square cavity, *Int. J. Heat Mass Transfer* **36**, 2899–2911 (1993).
18. Y. Jaluria and B. Gebhart, On transition mechanisms in vertical natural convection flow, *J. Fluid Mech.* **66**, 309–337 (1974).